arXiv:astro-ph/0406020v1 1 Jun 2004

Draft version from February 19, 2022, Accepted for ApJ Letter

SMA multi-line observations of the massive star-forming region IRAS 18089-1732

H. Beuther[1], Q. Zhang[1], T. Hunter[1], T.K. Sridharan[1], J.-H. Zhao[1], P. Sollins[1], P.T.P. Ho[1,2], S.-Y. Liu[2], N. Ohashi[2], Y.N. Su[2], J. Lim[2]

ABSTRACT

Submillimeter Array (SMA) observations of the high-mass star-forming region IRAS 18089-1732 in the 1mm and 850 m band with 1 GHz bandwidth reveal a wealth of information. We present the observations of 34 lines from 16 different molecular species. Most molecular line maps show significant contributions from the outflow, and only few molecules are confined to the inner core. We present and discuss the molecular line observations and outline the unique capabilities of the SMA for future imaging line surveys at high spatial resolution.

Subject headings: star: formation { submillimeter { techniques: interferometric { astrochemistry { line: identification { ISM: individual(IRAS 18089-1732)

1. Introduction

(Sub-)millimeter Interferometry offers great opportunities to study massive star-forming regions in detail. High-mass star formation proceeds in a clustered mode, and at the typical distances of a few kpc high angular resolution is necessary to resolve the different phenomena taking place. Furthermore, massive star-forming cores emit strongly in the (sub-)mm regime and exhibit a forest of molecular line transitions tracing various physical aspects (e.g., Schilke et al. 1997). Here, we present early results obtained in the field of massive star formation with the Submillimeter Array (SMA[1]) on Mauna Kea/Hawaii. Before the advent of the

[1]Harvard-Smithsonian Center for Astrophysics, 60 Garden Street, Cambridge, MA 02138

[2]Academia Sinica Institute of Astronomy and Astrophysics, No.1, Roosevelt Rd, Sec. 4, Taipei 106, Taiwan, R.O.C.

[1]The Submillimeter Array is a joint project between the Smithsonian Astrophysical Observatory and the Academia Sinica Institute of Astronomy and Astrophysics, and is funded by the Smithsonian Institution and the Academia Sinica.

SMA, the only sub-mm interferometry ever conducted was single-baseline work with the JCMT and CSO, which aimed largely at low-mass sources because the expected structures would be simple (e.g., Brown et al. 2000).

The target source IRAS 18089–1732 is part of a sample of 69 High-Mass Protostellar Objects selected mainly via infrared color-color criteria and the absence of strong cm continuum emission (Sridharan et al. 2002). It is approximately at a distance of 3.6 kpc[2] and its bolometric luminosity is about $10^{4.5}$ $L_\odot$ (Sridharan et al. 2002). Previous Millimeter continuum observations reveal a massive core $> 2000 M_\odot$ with H_2O and CH_3OH maser emission, and a weak 1 mJy cm source is detected (Beuther et al. 2002b,d). As part of a single-dish CO outflow study, wing emission indicative of molecular outflows was detected (Beuther et al. 2002c), and Sridharan et al. (2002) report the detection of the hot-core molecules CH_3CN and CH_3OH. Comprising all features of a young luminous massive star-forming region at an early evolutionary stage just beginning to form a hot core, IRAS 18089–1732 is an ideal target for early science with the SMA. While this letter focuses on the multi-line observations of IRAS 18089–1732, an accompanying letter discusses the (sub-)mm continuum and SiO/$HCOOCH_3$ line data revealing the disk-jet system (Beuther et al., this volume).

2. The Submillimeter Array (SMA)

IRAS 18089–1732 was observed with the SMA between May and July 2003 in two different configurations with 3 to 5 antennas in the array[3]. The phase reference center of the observations was R.A.[J2000] 18:11:51.4 and Dec.[J2000] –17:31:28.5. The projected baselines ranged from 10.8/18.6 to 120 m for the 1.3 mm/850 μm observations, respectively. For bandpass calibration we used the planet Mars. The flux density scale was derived by observations of the planet Uranus and is estimated to be accurate within 25%. Phase and amplitude calibration was done via frequent observations of the quasar NRAO 530, approximately 10° from the target source (S_{217GHz} 2.4 Jy and S_{354GHz} 1.5 Jy). The zenith opacity for the 350 GHz observations – measured at 225 GHz with the NRAO tipping radiometer operated by the CSO ((354 GHz) 3.2 (225 GHz)) – was excellent for one track ((354 GHz) 0.19) but somewhat worse for the second track ((354 GHz) 0.32). The data of the second track could only be used for the 850 μm continuum because the signal-to-noise

[2] The kinematic distance ambiguity is solved by associating the region via the near- and mid-infrared surveys 2MASS and MSX on larger scales with sources of known distance (Bontemps, priv. comm.).

[3] For more details on the SMA and its specifications see Ho, Moran & Lo (this volume) and the SMA web-site: http://sma-www.harvard.edu/.

ratio in the line data was too low. For the 217 GHz observations the opacity was slightly higher with (225 GHz) 0.12 in one night and (225 GHz) 0.3 in the other night. The doppler-tracking center frequency on the source was $v_{lsr} = 33.8$ km s^{-1}. The receivers operate in a double-sideband mode (DSB) with an IF band of 4–6 GHz. The correlator bandwidth at the time of observation was 1 GHz, and the frequency resolution was 0.825 MHz. In the 850 m band we tuned the receivers to the HCN (4–3) line at 354.5055 GHz in the upper sideband. At 1 mm the tuning was centered on the SiO (5–4) line at 217.1049 GHz in the lower sideband. Because of double-sideband reception we obtained simultaneously data at 344 GHz and 227 GHz. The beam sizes of the combined datasets at 1.3 mm was $2.7'' \times 1.7''$ and at 850 m $1.4'' \times 0.9''$ (uniform weighting), the beam size of the 850 m line data using only one track was $1.6'' \times 0.7''$. System temperatures (DSB) in the 850 m band were between 300–900 K and in the 1 mm band around 200 K. The primary beam at 217 GHz was $58''$ and at 354 GHz $36''$. The continuum rms was 7 mJy at 217 GHz and 40 mJy at 345 GHz. The calibration was done with the IDL superset MIR developed originally for OVRO and adapted for the SMA. The imaging was performed in MIRIAD.

3. Results

Detection of many molecular lines: Figure 1 presents two spectra taken at 217 GHz and 344 GHz (both on baselines of 25 m), showing an impressive line forest of various molecular lines. In the whole dataset with a total bandwidth of 4 GHz (1 GHz in a DSB mode per frequency setup) we detect 34 molecular lines from 16 molecules/isotopomers, with 5 lines remaining unidentified (Table 1). We detected lines from molecular species tracing various physical and chemical processes within massive star-forming regions. While silicon and sulphur bearing molecules are known to be strong in shocked regions and thus often trace molecular outflows, we also detected typical hot core molecules like CH_3OCH_3, CH_3OH, and numerous $HCOOCH_3$ lines. The data are rich in nitrogen bearing species as HCN, HC_3N, and $HC^{15}N$, which are subject to a different chemistry than, e.g., oxygen bearing species (e.g., Wyrowski et al. 1999). Furthermore, we observed the deuterated species DCN which again is subject to different chemical networks (e.g., Hatchell et al. 1998). It should be noted that the setup was chosen originally for SiO (5–4) and HCN (4–3), the other line detections were achieved because of the broad bandwidth. Transitions of other typical molecules like CH_3CN or CN were absent in this specific setup. The data suggest that because of the richness of lines in the (sub-)millimeter window, the SMA will almost always be able to sample many transitions simultaneously. Figure 1 also shows the different continuum levels at 1 mm and 850 m of which a detailed analysis is presented in the accompanying letter (Beuther et al., this volume). We estimate the line contamination to the broadband continuum flux in the

1.3mm band and the 850 m band both to be about 10% .

Comparing the line forest with Orion-KL, the proto-typical high-mass star-forming region toward which many line surveys have been conducted (e.g., Sutton et al. 1985; Schilke et al. 1997), we detect in the same frequency ranges all lines previously observed toward Orion-KL, but with on average significantly narrower line width toward IRAS 18089–1732: e.g., toward Orion-KL in the 344 GHz band the $HC^{15}N$ and CH_3OCH_3 blend into the broad line wings of the SO line (Schilke et al. 1997) whereas they are clearly resolved from each other in the IRAS 18089–1732 data (Fig. 1). The two main reasons likely contributing to this difference are the larger luminosity of Orion (10^5 L compared to $10^{4.5}$ L) and the earlier evolutionary stage of IRAS 18089–1732 which is just at the verge of forming a hypercompact HII region (Sridharan et al. 2002).

The large number of observed $HCOOCH_3$ lines allows us to estimate a temperature for the central region (Oesterling et al. 1999). As the data quality is not good enough to image all lines properly, especially in the 850 m band (see §3), we fitted the intensities in the visibility domain. From a boltzmann plot we derive a rotation temperature of 350 100 K. As $HCOOCH_3$ traces the dense gas at the core center, this rather high temperature indicates the existence of a hot molecular core in the near vicinity of the central hypercompact HII region (Beuther et al. 2002d). Such high temperatures at the core center are further supported by recent VLA detections of the NH_3(6,6) line with an energy level of 412 K.

Simultaneous imaging: Many of the presented molecular lines are strong enough to image, which is an enormous step forward compared to single-dish line surveys. Single-dish observations rarely have sufficient angular resolution to resolve the sources, although massive star-forming regions are usually so complex that the chemistry, density and temperatures exhibit detailed spatial structures. Simultaneous interferometric imaging of various molecular lines is thus the best tool to investigate these characteristics in more detail (e.g., Wilner et al. 1994; Wright et al. 1996; Blake et al. 1996; Wyrowski et al. 1999).

Because we have only one track at 850 m with good enough signal-to-noise ratio to use for the line imaging, we are restricted in this band to the two strongest lines: HCN and SO (Figure 2). In the 1mm band we could image many more lines. Figure 2 presents a characteristic subset of the integrated emission maps, consisting of the outflow tracer SiO, the hot-core tracer $HCOOCH_3$, the molecule CH_3OH, the sulphur bearing molecule H_2S, the deuterated molecule DCN and the nitrogen bearing molecule HC_3N. Table 1 presents the peak and integrated fluxes S_{peak} & S. Individual characteristics of the different species are discussed below. In the accompanying paper (Beuther et al., this volume), we discuss the SiO (5–4) and $HCOOCH_3$ (20–19) line observations of this dataset in detail. Here we present only the integrated SiO and $HCOOCH_3$ emission to outline their outflow/core properties

and to associate the emission of the other molecules with the different physical components within the region.

4. Discussion

As shown in Fig. 2 and outlined in Beuther et al. (this volume), the SiO (5–4) data depict an outflow emanating from the central dust core in the northern direction. This outflow is approximately in the plane of the sky and the SiO emission traces only the northern lobe. The hot core molecule $HCOOCH_3$ (20–19) traces the central dust condensation with a velocity gradient across the core at a position angle of 35 with respect to the outflow direction. That the $HCOOCH_3$ velocity gradient is not exactly perpendicular to the outflow can be interpreted as a rotating gas and dust disk which is influenced by the outflow as well as possible infall.

To give a flavor of the velocity structures varying with molecular line, Figure 3 shows two examples of channel maps, with CH_3OH tracing the core and H_2S tracing the outflow. The line-width of the two molecules is not very different because the outflow is approximately in the plane of the sky. However, the spatial distribution varies significantly. The core-tracing CH_3OH shows a similar east-west velocity shift as $HCOOCH_3$ whereas the H_2S emission extends to the north comparable to SiO. As the line-widths of the various molecules are of the same order we base the following outflow/core associations mainly on morphological similarities. Comparing the molecular line data shown in Figure 2 with the results from the SiO/$HCOOCH_3$ observations, we find that many lines are influenced by the outflow. Most prominently, this influence is observed in the sulphur bearing species H_2S and SO. However, we find extensions to the north also in DCN and HCN, and, although to a lesser degree, in HC_3N. CH_3OH appears to be least affected by the outflow. Quantitatively speaking, we compare the source sizes within the 10% levels of the peak emission and the ratio of integrated to peak flux presented in Table 1. Taking into account the higher angular resolution and the larger interferometric spatial filtering in the 850 m band, $HCOOCH_3$, CH_3OH and HC_3N are rather compact whereas the other molecules are more extended. This is reflected in the lower integrated to peak flux ratios of the core-tracing molecules.

These findings are less of a surprise for H_2S and SO, which are known to be released from dust grains in shock interactions with molecular jets and outflows (e.g., Bachiller et al. 2001). In contrast, species like HCN and HC_3N were believed to be mainly hot core tracing molecules (Wyrowski et al. 1999). Especially, HCN was considered as a possible disk tracer in massive star formation, which is not the case in IRAS 18089–1732 because the outflow significantly shapes the overall HCN emission. Similarly, recent observations toward IRAS 18566+0408

and IRAS 20126+4104 reveal strong HCN emission toward its outflow (Zhang, priv. comm.). The 354 GHz HCN (4–3) data need to be improved for a more detailed investigation of HCN outflow and core emission in IRAS 18089–1732. On first sight, one gets the impression that the DCN emission might be more extended than HCN, but this is mainly due to the different frequency bands and thus varying interferometric spatial filtering. Therefore, we re-imaged the DCN data using a short baseline cutoff as given by the HCN observations (22 k), and we find that the spatial distribution of HCN and its deuterated species DCN is quite similar. The compact CH_3OH emission exhibits an east-west velocity gradient similar to $HCOOCH_3$ (20–19). However, CH_3OH has been observed to be associated with outflows in other sources (e.g., Beuther et al. 2002a). Thus, its emission is not always unambiguously confined to core emission and has to be treated with similar caution as HCN.

The data shown in this letter outline the unique capacities of the SMA in performing imaging spectral line surveys. The presented data were taken in summer time in a testing mode with the partially completed SMA. Therefore, using the full capabilities of the SMA in the very near future (e.g., doubled bandwidth of 2 GHz, 8 antennas within the array, 2 receivers simultaneously, see also Ho et al., this volume) we will get a far better sensitivity and imaging quality for forthcoming physical and chemical studies of various astrophysical objects.

We like to thank the whole SMA staff for making this instrument possible! H.B. acknowledges financial support by the Emmy-Noether-Program of the Deutsche Forschungsgemeinschaft (DFG, grant BE 2578/1).

REFERENCES

Bachiller, R., Perez Gutierrez, M., Kumar, M.S.N., & Tafalla, M. 2001, A&A, 372, 899

Beuther, H., Schilke, P., Gueth, F., et al. 2002a, A&A, 387, 931

Beuther, H., Schilke, P., Menten, K.M., et al. 2002b, ApJ, 566, 945

Beuther, H., Schilke, P., Sridharan, T.K., et al. 2002c, A&A, 383, 892

Beuther, H., Walsh, A., Schilke, P., et al. 2002d, A&A, 390, 289

Blake, G.A., Mundy, L.G., Carlstrom, J.E., et al. 1996, ApJ, 472, L49+

Brown, D.W., Chandler, C.J., Carlstrom, J.E., et al. 2000, MNRAS, 319, 154

Hatchell, J., Millar, T. J., & Rodgers, S. D. 1998, A&A, 332, 695

Oesterling, L. C., Albert, S., de Lucia, F. C., Sastry, K. V. L. N., & Herbst, E. 1999, ApJ, 521, 255

Schilke, P., Groesbeck, T. D., Blake, G. A., & Phillips, T. G. 1997, ApJS, 108, 301

Sridharan, T. K., Beuther, H., Schilke, P., Menten, K. M., & Wyrowski, F. 2002, ApJ, 566, 931

Sutton, E. C., Blake, G. A., Masson, C. R., & Phillips, T. G. 1985, ApJS, 58, 341

Wilner, D. J., Wright, M. C. H., & Plambeck, R. L. 1994, ApJ, 422, 642

Wright, M. C. H., Plambeck, R. L., & Wilner, D. J. 1996, ApJ, 469, 216

Wyrowski, F., Schilke, P., Walmsley, C. M., & Menten, K. M. 1999, ApJ, 514, L43

This preprint was prepared with the AAS LaTeX macros v5.2.

Table 1. Observed lines

Line	GHz	S^{b}_{peak} $\frac{Jy}{beam}$	$S^{b,c}$ Jy	Size[c] ″	$\frac{S}{S_{peak}}^{d}$
SO_2 $22_{2,20}$ – $22_{1,21}$	216.643				
H_2S $2_{2,0}$ – $2_{1,1}$	216.710	2.3	6.4	39.7	0.6
$HCOOCH_3$ 18–17	216.839				
CH_3OH 4_2 – 5_1	216.946	2.0	2.8	20.5	0.3
$HCOOCH_3$ 20–19	216.966	2.1	2.3	15.9	0.2
SiO 5–4	217.105	1.0	2.6	31.9	0.6
UL[a]	217.193				
DCN 3–2	217.239	1.9	4.3	32.6	0.5
UL[a]	217.300				
UL[a]	217.400				
$HCOOCH_3$ 19–18 E	227.020				
$HCOOCH_3$ 19–18 A	227.028				
HC_3N 25–24	227.419	3.4	5.9	21.3	0.4
$HCOOCH_3$ 21–20	227.562				
UL[a]	227.815				
$HCOOCH_3$ 27–26 E	343.732				
CH_3OCH_3 17–16	343.753				
$HCOOCH_3$ 27–26 A	343.758				
H_2CS $10_{2,8}$ – $9_{2,7}$	343.811				
$OC^{34}S$ 29–28	343.983				
$HCOOCH_3$ 32–31	344.030				
CH_2OH–E	344.110				
$HC^{15}N$ 4–3	344.200				
SO 8_8 – 7_7	344.311	2.4	4.2	5.6	1.5
CH_3OCH_3 19–18	344.358				
CH_3OH $19_{10,9}$ – $18_{10,8}$	344.445				
CH_3OCH_3 11–10	344.512				
$^{34}SO_2$ $19_{1,19}$ – $18_{0,18}$	344.581				
UL[a]	354.129				
$^{13}CH_3OH$ 4_3 – 3_2	354.446				

Table 1 | Continued

Line	GHz	S^{b}_{peak} $\frac{Jy}{beam}$	$S^{b,c}$ Jy	Size[c] 00 2	$\frac{S}{S_{peak}}^{d}$
HCN (0,1,0) 4–3	354.461				
HCN 4–3	354.506	2.2	3.1	4.9	1.3
$HCOOCH_3$ 33–32	354.608				
HC_3N 39–38	354.699				

[a]Unidentified line

[b]Errors of the fluxes are within the calibration uncertainty of 25%.

[c]Integrated flux and size within the 10% level of the peak emission

[d]To reduce differences between the two bands (different beams and spatial sampling) this ratio is divided by the beam.

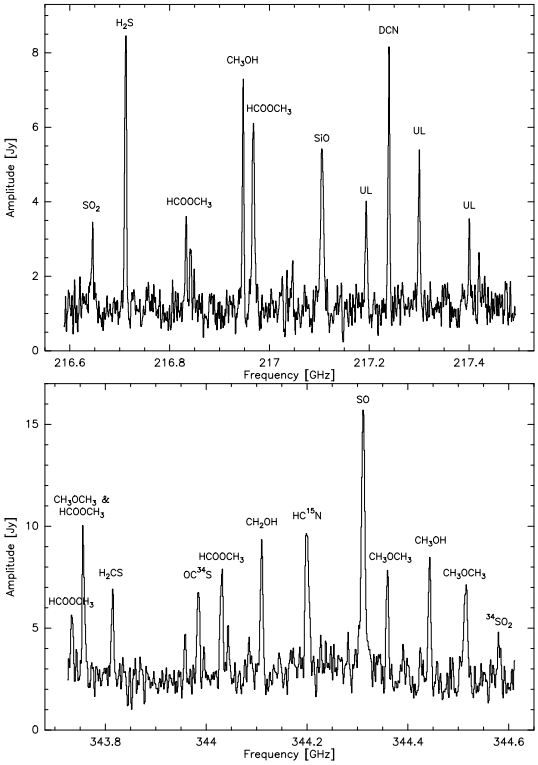

Fig. 1.— SMA spectra toward the high-mass star-forming region IRAS 18089–1732. The spectrum on top is taken at 217 GHz and the bottom one at 344 GHz, both with baseline length of approximately 25 m and a bandwidth of 1 GHz. The other sidebands at 227 GHz and 354 GHz are not shown. No continuum subtraction has been performed to show the different continuum levels in the two bands consistent with dust emission (see the accompanying paper by Beuther et al., this volume). UL marks unidentified lines.

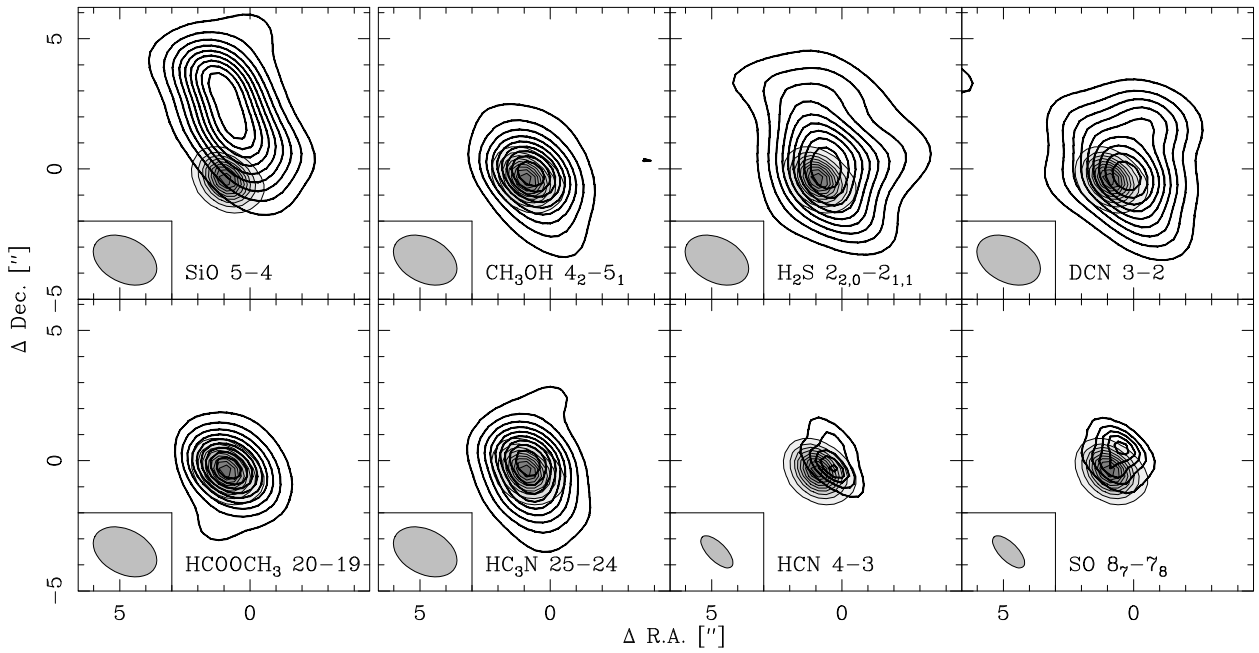

Fig. 2.| Integrated line intensity images of various molecular transitions toward IRAS 18089-1732 are shown as thick contours. The grey-scale and thin contours present the 850 m continuum image (see also Beuther et al., this volume). The molecules are labeled, and the beams are shown at the bottom left corner of each panel. The continuum and the 1mm line images are contoured in 10% level steps from the integrated intensities presented in Table 1. Line images of HCN and SO are contoured from 10 to 90% in 20% steps.

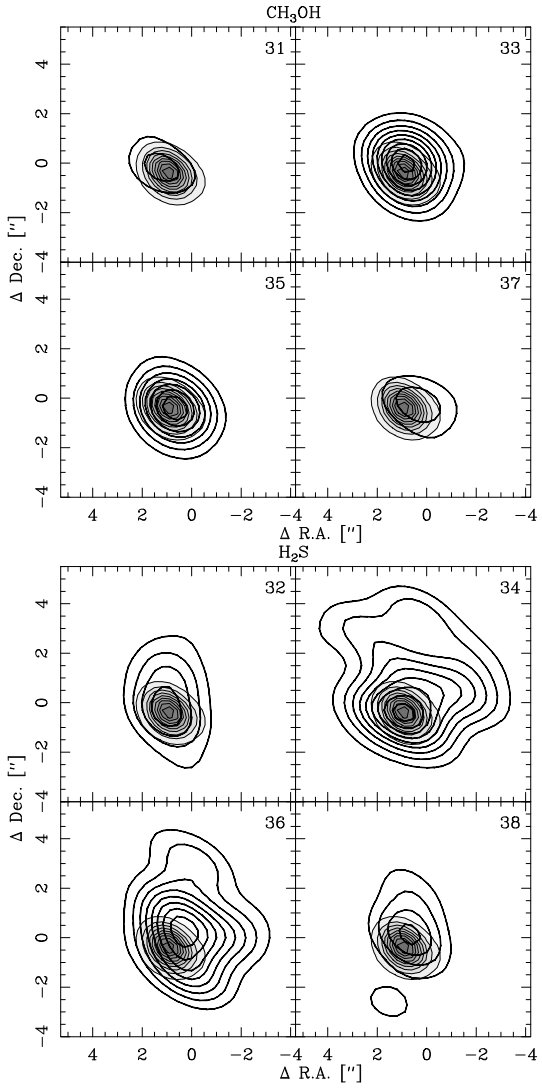

Fig. 3.— Channel maps of CH_3OH and H_2S. The grey-scale and thin contours present the 850 μm continuum image, the thick contours show the line emission. The continuum is contoured in 10% steps from the peak intensity, and the channel maps are contoured from 15 to 95% (10% steps) from the integrated intensity in the strongest channel, respectively. The v_{lsr} velocity of each channel is marked at the top-right of each panel.